analytical chemistry

Article

pubs.acs.org/ac

Dynamic Self-Referencing Approach to Whispering Gallery Mode Biosensing and Its Application to Measurement within Undiluted Serum

Tess Reynolds,[*,†] Alexandre François,[†,‡] Nicolas Riesen,[†] Michelle E. Turvey,[§] Stephen J. Nicholls,[∥] Peter Hoffmann,[†,§] and Tanya M. Monro[†,‡]

[†]The Institute for Photonics and Advanced Sensing (IPAS) and [§]Adelaide Proteomics Centre, University of Adelaide, Adelaide SA 5005, Australia

[‡]University of South Australia, Adelaide SA 5000, Australia

[∥]South Australian Health and Medical Research Institute (SAHMRI), University of Adelaide, Adelaide SA 5000, Australia

ABSTRACT: Biosensing within complex biological samples requires a sensor that can compensate for fluctuations in the signal due to changing environmental conditions and nonspecific binding events. To achieve this, we developed a novel self-referenced biosensor consisting of two almost identically sized dye-doped polystyrene microspheres placed on adjacent holes at the tip of a microstructured optical fiber (MOF). Here self-referenced biosensing is demonstrated with the detection of Neutravidin in undiluted, immunoglobulin-deprived human serum samples. The MOF allows remote excitation and collection of the whispering gallery modes (WGMs) of the microspheres while also providing a robust and easy to manipulate dip-sensing platform. By taking advantage of surface functionalization techniques, one microsphere acts as a dynamic reference, compensating for nonspecific binding events and changes in the environment (such as refractive index and temperature), while the other microsphere is functionalized to detect a specific interaction. The almost identical size allows the two spheres to have virtually identical refractive index sensitivity and surface area, while still having discernible WGM spectra. This ensures their responses to nonspecific binding and environmental changes are almost identical, whereby any specific changes, such as binding events, can be monitored via the relative movement between the two sets of WGM peaks.

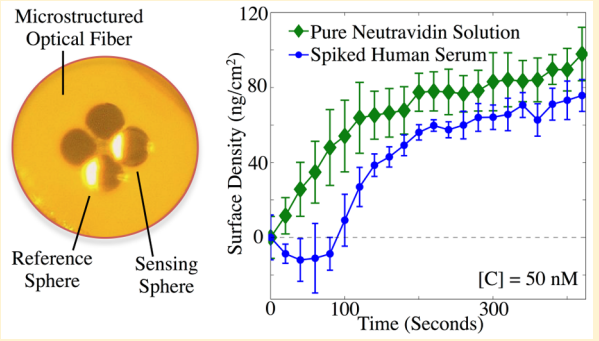

The phenomenon of whispering gallery modes (WGMs) within microresonators as a label-free sensing modality has emerged as a powerful contender for biosensing and medical diagnostic applications.[1,2] It has enabled unprecedented detection limits down to single molecules,[3] and has given way to new in vivo sensing opportunities.[1,4,5] The spectral positions of the WGMs are determined by both the properties of the resonator (e.g., diameter, shape, refractive index) as well as the surrounding medium. The latter feature allows changes in the environment to be monitored via shifts in the spectral positions of the resonances. Surface functionalization of the resonator can also be utilized allowing specific interactions with desired target analytes such as proteins,[6,7] bacteria,[8] and DNA[9,10] to be monitored within pure samples in controlled laboratory conditions.

However, the ability of a sensor, and in particular a label-free biosensor, to distinguish or eliminate unwanted fluctuations in the signal due to variations in, for example, temperature, surrounding refractive index, or nonspecific binding (NSB) is critical in real clinical samples. While it is usually possible to control the environmental conditions, such as temperature, reducing the effect of unwanted binding events in clinical samples is far more challenging. Different methods to overcome this critical issue have been proposed, all based on surface chemistry approaches, using, for example, NHS esters,[11] CM dextran,[12] or polyethylene glycol (PEG).[13,14] Integrating PEGs with silica microsphere resonators has, for example, allowed thrombin (~8 μM) to be detected in 10-fold diluted human serum inside a flow cell.[7] However, this method requires serum to be diluted, which adds an additional processing step and reduces the concentration of the analyte by the same factor, increasing the demands on the performance of the sensor. For some applications, such as the early diagnosis of myocardial infarctions in cardiology, for example, where the analyte concentration is already very small,[15−17] this technique might not be suitable and alternative approaches have to be found. One such approach is to design a self-referencing sensor that allows both environmental changes and NSB events to be compensated, as is presented here.

A relatively straightforward approach of developing a self-referencing sensor is to introduce a second resonator that serves

Received: January 27, 2016
Accepted: February 26, 2016

DOI: 10.1021/acs.analchem.6b00365
Anal. Chem. XXXX, XXX, XXX−XXX

as a dynamic reference, similar to multiplexed sensing techniques.[18] Multiplexing of WGM sensors has previously been proposed conceptually[18] and demonstrated in a range of resonator geometries and configurations including passive microspheres,[9] microdisks,[19] and liquid core ring resonators[20] and fluorescent microspheres.[21,22] Fluorescent or active resonators are particularly interesting in this context, as they allow remote excitation of the resonator, thereby alleviating some of the practical limitations of passive resonator configurations.[9,23−25] Active resonators do display lower *Q*-factors[26] in comparison with passive resonators,[27,28] however, techniques exist that can improve the *Q*-factor, such as operating the resonator within the stimulated emission regime[29] or breaking the symmetry of the resonator by placing it onto the tip of a microstructured optical fiber (MOF).[30] This second technique has the additional advantage of creating a robust and easy to use dip-sensing architecture.[1]

In this study we demonstrate a self-referenced WGM biosensing platform for the specific detection and quantification of biomolecules in undiluted human serum. Our self-referenced sensing platform is an extension of our previously reported dip sensing active WGM platform using a 4-hole silica MOF which allows for the remote excitation and collection of the WGM signal from a dye-doped polystyrene microsphere placed in one of the holes at the tip of the fiber.[1] A second, almost identical microsphere (reference resonator), but differing in its surface chemistry from the sensing microsphere, is placed in an adjacent hole acting as a dynamic reference, Figure 1A. The reference

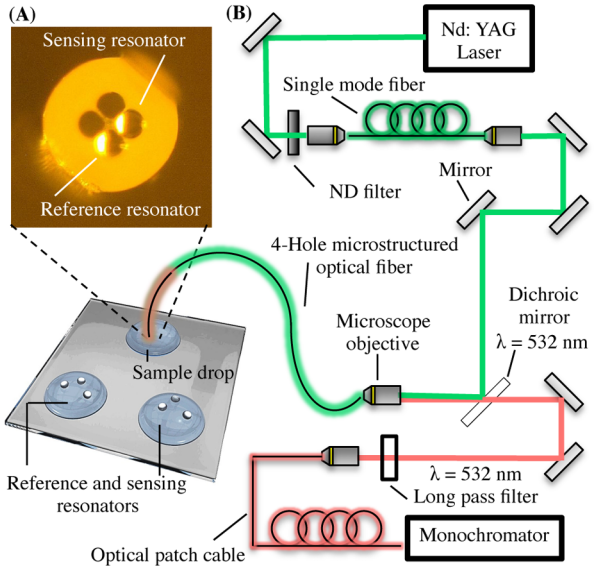

Figure 1. (A) Bright-field microscope image of two 15 μm diameter dye-doped polystyrene microspheres positioned onto the tip of a 4-hole microstructured optical fiber (MOF). (B) Schematic of the optical setup.

resonator compensates for nonspecific binding as well as environmental changes, acting as a dynamic reference, while the first sphere (sensing resonator) is functionalized for detecting a specific analyte. Due to the highly sensitive nature of the resonance wavelength positions to the resonator's effective radius, differences of only nanometers allows the spectrum of each individual sphere to be clearly distinguished. The nearly identical size of the resonators also guarantees that the two spheres have virtually identical refractive index sensitivity and surface area, so their response to any environmental changes or NSB is almost identical, while the proximity of the spheres on the MOF's tip allows them to simultaneously experience the same local environment. Furthermore, utilizing a single gain medium for both spheres ensures that the sensing performance (sensitivity and resolution) of both resonators remain comparable, allowing the use of the relative displacement between the two sets of peaks for tracking specific binding events.

To evaluate the performance of our self-referenced fiber tip sensing platform we used a well-known specific interaction model based on biotin-Neutravidin. The Neutravidin detection limit in buffer solution (PBS) was first characterized and then repeated in Neutravidin spiked undiluted, immunoglobulin-deprived human serum samples. Following from our previous work,[1] the measurements were performed in static conditions, by simply dipping the MOF tip with attached microsphere resonators into the different liquid samples, as shown in Figure 1B. In both sets of measurements, the nonspecific binding signal was monitored using the reference resonator, while the total contribution of specific and nonspecific interactions was measured using the sensing resonator. The relative movement between the two sets of resonances was then monitored.

EXPERIMENTAL SETUP, MATERIALS, AND METHOD

The polystyrene microspheres (nominal diameter of 15.00 ± 1.43 μm from Polyscience Inc.) were doped with the fluorescent dye Nile Red (λ_{ex} = 532 nm, λ_{em} = 590 nm)[31] using a liquid two-phase system.[32] Following this process, the microspheres were annealed and rinsed thoroughly to remove any trace of the organic solvent (xylene) used during the doping process, eliminating any potential drift of the resonance positions over time. The surface functionalization begins with the deposition of a series of positively and negatively charged polyelectrolyte layers, polyallylamine hydrochloride (PAH) and polystyrene sulfonate (PSS),[33] to form three layers (PAH/PSS/PAH).[1] The microspheres were then separated into two batches, sensing and reference resonators, with only the sensing resonator batch being biotinylated for monitoring the specific interaction with Neutravidin. For the sensing resonators, the primary amine of the PAH layer was used to covalently immobilize biotin-D using a solution of 1-ethyl-3-(3-dimethylamionpropyl) carbodimide (EDC) and *N*-hydroxysuccinimide (NHS) as coupling reagents. As a final process, both the reference and the sensing resonators were incubated in 2.5% casein solution for 24 h to cover nonspecific binding sites.

A schematic of the optical setup is shown in Figure 1B, where a frequency-doubled YAG laser (λ = 532 nm, ~800 ps pulse duration, 10 kHz repetition rate) was used for the excitation of the active microspheres beyond their lasing thresholds, enabling higher *Q*-factors, as previously shown.[32] The light from the YAG was spatially filtered using a tapered single mode fiber (SMF28 $Ø_{core}$ = 4 μm) before being coupled into the 4-hole silica MOF ($Ø_{core}$ = 7 μm, $Ø_{hole}$ ~ 15 μm) shown in Figure 1A. The WGM emission from the microspheres is then recaptured by the MOF and directed back through a dichroic mirror into a monochromator equipped with a cooled CCD (2048 pixels) where the WGM spectrum is recorded.

To attach a microsphere to the tip of the MOF a drop of water containing the microspheres was placed on top of a glass coverslip and positioned on an inverted microscope. A three-axis translational stage was used to hold and align the tip of the MOF as it was carefully lowered down into the drop of microspheres.

DOI: 10.1021/acs.analchem.6b00365
Anal. Chem. XXXX, XXX, XXX−XXX

After recording the emission spectra of free floating microspheres from both the sensing and reference resonator batches, using free-space excitation and collection, one microsphere was selected from each droplet and brought into contact with the fiber tip. Due to the hydrophobic nature of both the MOF tip and the microspheres, the microspheres can easily be positioned in individual holes of the MOF, as seen in Figure 1A. It is important to note that once attached to the MOF tip, the microspheres stay in place and can be easily manipulated and dipped into other liquid droplets.

DATA ANALYSIS

All the binding kinetics presented here are presented in terms of the change in surface density of adsorbed molecules onto the surface of the resonator (d, ng/cm^2). This value can be estimated from the wavelength shift $\Delta\lambda$, through the effective radius increase ΔR using the following equations,[34] where λ is the initial resonance wavelength, R is the initial resonator radius which can be calculated from the spacing of successive modes with the same polarization using eqs 2 and 3, e is the thickness of the deposited layer, and n_L and n_s are the refractive indices of the layer and sphere, respectively. By fitting Gaussian functions to the resonance peaks, the spectral position of an initial resonance wavelength λ, and subsequent positions of the peak over time can be determined.

$$\frac{\Delta\lambda}{\lambda} = \frac{\Delta R}{R} = \frac{n_L e}{n_s R} \tag{1}$$

$$R = \frac{\lambda_{m+1} m}{2\pi n_s} \tag{2}$$

$$m = \frac{\lambda_{m+1}}{\lambda_m - \lambda_{m+1}} + 1 \tag{3}$$

where m is the azimuthal mode number and λ_{m+1} and λ_m are the wavelengths of two successive modes with the same polarization.

$$d = \frac{M}{N_A \sigma_p^{-1}} \tag{4}$$

$$\sigma_p^{-1} = \frac{n_s}{n_m} \frac{\alpha_{ex}}{\varepsilon_0 (n_s^2 - n_m^2)} \frac{1}{\Delta R} \tag{5}$$

$$\alpha_{ex} = \frac{\varepsilon_r - 1}{\varepsilon_r + 2} \frac{3M\varepsilon_0}{N_A \rho_m} \tag{6}$$

Here, M is the molecular weight, N_A is Avogadro's number, σ_p is the projected area of the adsorbed molecule, α_{ex} is the excess polarizability, which to a first approximation can be calculated using the Clausius-Mossotti formula (eq 6), ε_0 is the free-space permittivity, ε_r is the dielectric function of the molecule considered, ρ is the mass density (ρ = 1.37 g/cm^3 for most proteins[35]) and n_m and n_s are the refractive indices of the surrounding environment and microsphere, respectively. Calculating the surface density allows comparison with other techniques and sensing geometries as it removes the dependence on the geometry as well as the refractive index sensitivity of the sensor being considered.

RESULTS AND DISCUSSION

Figure 2A and B show the typical WGM spectra of the two-microsphere system above and below the lasing threshold, respectively. Below the lasing threshold the resonances of the two spheres cannot be distinguished. However, operating the spheres above their lasing thresholds not only allows the spectrum of each individual sphere to be clearly identified, but also improves the resolution, enabling lower detection limits to be reached.[1] The resonance spectra typically do not overlap, when operated in the stimulated emission regime as even a minute deviation in diameter between the two microspheres results in a discrepancy between the resonances. In this configuration, the spheres can either be tracked individually by following an individual peak or alternatively, by performing a convolution on the two resonator comb-like WGM spectrum as both spheres respond to the same environment, Figure 2C.

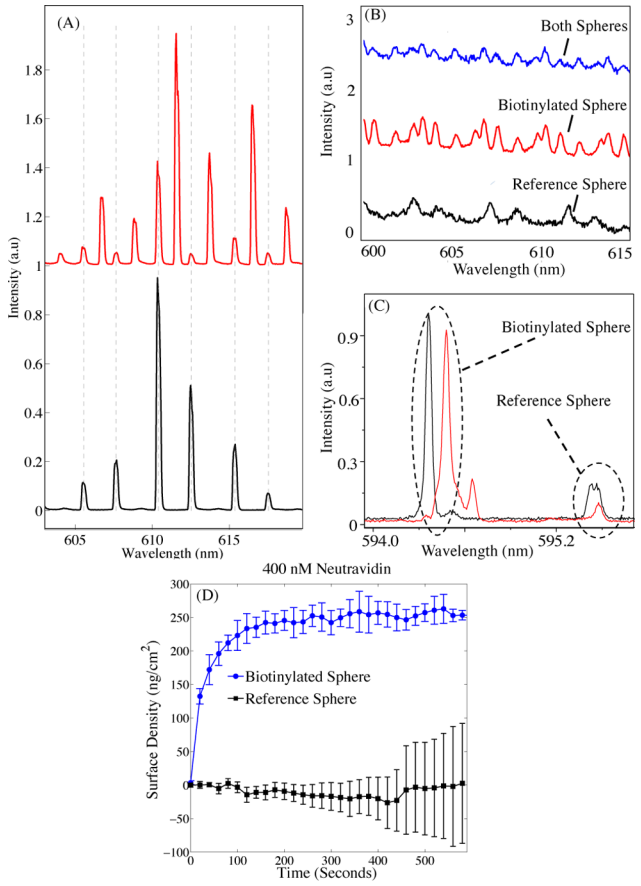

Figure 2. (A) Whispering gallery mode spectrum of the reference sphere alone (black trace) and both the biotinylated and reference spheres (red trace) attached to the tip of the microstructured optical fiber (MOF), operating above the lasing threshold. Both spheres are 15 μm in diameter. (B) Whispering gallery mode spectrum of the reference (black), biotinylated (red), and both the reference and biotin spheres, when attached to the tip of the microstructured optical fiber below the lasing threshold. (C) Comparison of the whispering gallery mode spectra of both the reference and biotinylated microspheres attached to the tip of the MOF when initially in water (black trace) and after dipping into Neutravidin solution for 8 min (red trace). (D) Binding kinetic of Neutravidin onto the biotinylated sphere (blue trace) and reference sphere (black trace).

Once both spheres were attached, spectra were taken at 20 s intervals as the fiber was moved into the Neutravidin solution. Figure 2D shows the response of both microspheres when placed in 400 nM Neutravidin solution. From the responses of the two spheres it is clear that binding is occurring on the biotinylated sphere, with equilibrium being reached after approximately 200 s, while the reference sphere spectrum remains relatively stable

DOI: 10.1021/acs.analchem.6b00365
Anal. Chem. XXXX, XXX, XXX−XXX

throughout the measurement with deviations toward the end of the measurement. This result is consistent with our previous demonstrations of fiber tip[1] and fluorescent microcapillary[36] sensing. We also note that the presence of the reference sphere does not have any effect on the biotinylated sphere's performance. As such, the process is repeated for decreasing Neutravidin concentrations, with 3 measurements made for each concentration. Each individual measurement was completed with a new set of spheres. No deviation was observed for the reference spheres during the Neutravidin measurements, and for simplicity only the binding kinetic of the biotinilated sphere is shown for each of the concentrations in Figure 3, where the error bars have been calculated from the standard deviation of all three trials completed for each concentration.

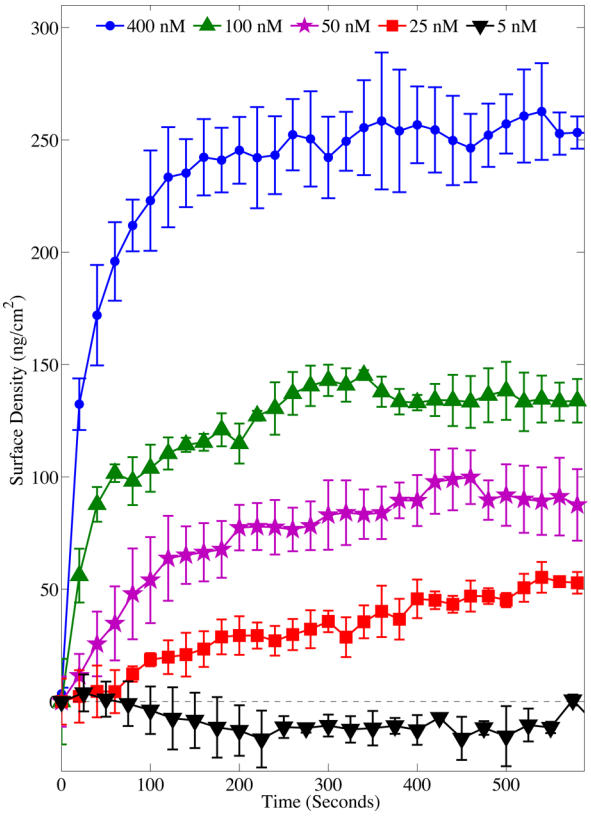

Figure 3. Binding kinetic of Neutravidin on a 15 μm biotinylated microsphere of five different concentrations 5−400 nM.

After completing these initial trials in PBS, the same experimental procedure was used to investigate the sensor's response in human serum samples. Drops of each of the sphere populations were once again placed on top of a glass coverslip, with a single sphere from each subsequently being attached to the fiber tip, along with 30 μL drops of 1:20 (v/v) and 1:40 (v/v) diluted human serum without Neutravidin added. The response of the individual spheres in the sensor is displayed in Figure 4. Examining Figure 4, it is clear that significant adsorption is occurring in both sphere populations, however there is a reduction in the adsorption of the biotinylated sphere as the dilution of the sample increases, Figure 4A, while the reference sphere's response remains almost unchanged, Figure 4B. Without any added Neutravidin in the diluted serum sample, these results indicate that there is another molecule present in the serum that is interacting and binding to the biotinylated sphere

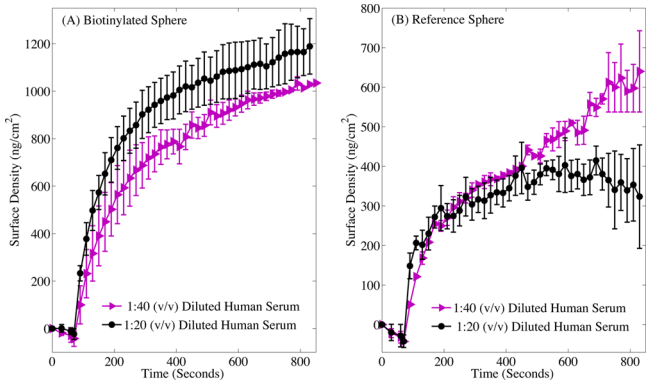

Figure 4. Binding kinetic of a sensing resonator (A) and reference resonator (B) attached to the tip of a fiber dipped into two human serum samples of different dilution.

surface. It has been reported that immunoglobulin can interact with biotin, resulting in false positive results for similar biotinylated-based immunoassays.[37]

Therefore, to avoid such false positive results while using biotin-Neutravidin as a specific interaction model, the immunoglobulin was removed from our serum samples by brief incubation and pull-down with protein A/G-conjugated sepharose beads. Four pull-downs with protein A/G beads were required to ensure that the false positive signal on the biotinylated microsphere was reduced to zero using undiluted serum while significant adsorption on the reference microsphere due to the nonspecific binding of the large protein content of the serum was still present.

Tests were repeated with pure human serum, with the immunoglobulin removed, avoiding the unwanted binding between the immunoglobulin and the sensing resonator, but spiked with a known Neutravidin concentration. The results for the lowest concentration tested are shown in Figure 5.

For all the tests performed, the reference resonator exhibited a similar behavior characterized by a sharp wavelength shift, or increase of the surface density, due to the large NSB component introduced by the serum, despite the use of casein as a blocking reagent. This highlights the fact that blocking solutions such as caseine, bovine serum albumin, and alike are inherently inefficient at preventing NSB in complex biological samples. The biotinylated microspheres, however, showed a steady increase in the surface density beyond the initial WGM wavelength shift due to the high refractive index of the serum, which characterizes the Langmuir adsorption of the Neutravidin onto the biotinylated resonator surface, down to 25 nM Neutravidin concentration. Once the contribution from the NSB is subtracted from the biotinylated microsphere response a perfect correlation between the Neutravidin binding kinetic in PBS and undiluted serum was reached as shown in the Figure 5D,E. For the lowest concentration tested (5 nM), no unambiguous positive detection of Neutravidin can be observed whether in PBS or undiluted serum.

In conclusion, this simple approach of using two almost identical microspheres, differing by their surface functionalization, for self-referencing purposes has shown that specific detection and quantification in undiluted serum samples can be realized. The reference microsphere allows for the compensation of the nonspecific binding, enabling the quantification of the binding of the analyte onto the sensing resonator surface in

DOI: 10.1021/acs.analchem.6b00365
Anal. Chem. XXXX, XXX, XXX−XXX

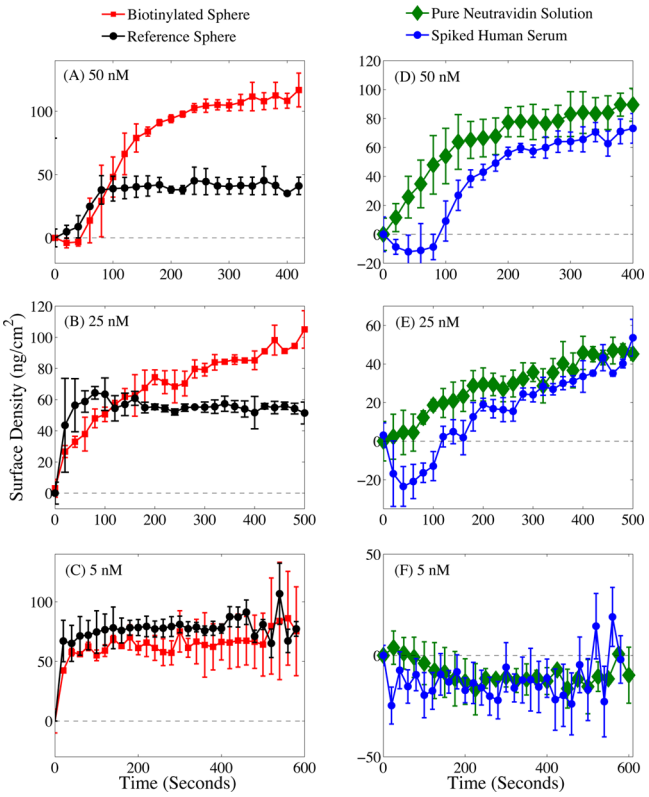

Figure 5. Individual sphere responses of the biotinylated (red trace) and reference (black trace) spheres when dipped into human serum samples spiked with (A) 50, (B) 25, and (C) 5 nM concentrations of Neutravidin. (D−F) Comparison of the corrected binding kinetic of the sensor in the spiked human serum samples (blue trace) with binding kinetic in the pure Neutravidin solution (green trace).

complex biological samples to be correlated with what happens with the same target analyte in buffer solution.

While for the sake of the specific interaction model used for this demonstration, the immunoglobulin had to be removed, one can appreciate that this approach can still be used for the detection of other more relevant biomolecules in serum, without having to process the serum by removing the immunoglobulin once antibodies are used to target a specific biomolecule instead of biotin. Furthermore, one can also expand this concept to multiplexed detection of different biomolecules simultaneously, taking advantage of the multiple holes on the MOF to accommodate microspheres targeting different biomolecules.

AUTHOR INFORMATION

Corresponding Author

*E-mail: tess.reynolds@adelaide.edu.au. Fax: +61-8-8313-4380.

Notes

The authors declare no competing financial interest.

ACKNOWLEDGMENTS

The authors acknowledge the support of T.M.M.'s ARC Georgina Sweet Laureate Fellowship. This work was performed in part at the Optofab node of the Australian National Fabrication Facility utilizing Commonwealth and SA State Government funding. Authors thank Roman Kostecki, Erik Schartner, Peter Henry, and Alastair Dowler for help with the silica microstructured fiber fabrication.

REFERENCES

(1) François, A.; Reynolds, T.; Monro, T. M. *Sensors* **2015**, *15*, 1168−1181.
(2) Agarwal, M.; Teraola, I. *Anal. Chem.* **2015**, *87*, 10600−10604.
(3) Baaske, M. D.; Foreman, M. R.; Vollmer, F. *Nat. Nanotechnol.* **2014**, *9*, 933−939.
(4) Humar, M.; Yun, S. H. *Nat. Photonics* **2015**, *9*, 572−576.
(5) Schubert, M.; Steude, A.; Liehm, P.; Kronenberg, N. M.; Karl, M.; Campbell, E. C.; Powis, S. J.; Gather, M. C. *Nano Lett.* **2015**, *15*, 5647−5652.
(6) Ballard, Z.; Baaske, M. D.; Vollmer, F. *Sensors* **2015**, *15*, 8968−8990.
(7) Pasquardini, L.; Berneschi, S.; Barucci, A.; Cosi, F.; Dallapiccola, R.; Insinna, M.; Lunelli, L.; Conti, G. N.; Pederzolli, C.; Salvadori, S.; Soria, S. *J. Biophotonics* **2013**, *6*, 178−187.
(8) Anderson, M. E.; O'Brien, E. C.; Grayek, E. N.; Hermansen, J. K.; Hunt, H. K. *Biosensors* **2015**, *5*, 562−576.
(9) Vollmer, F.; Arnold, S.; Braun, D.; Teraoka, I.; Libchaber, A. *Biophys. J.* **2003**, *85*, 1974−1979.
(10) Fan, X. D.; Sutter, J. D.; White, I. M.; Zhu, H. Y.; Shi, H. D.; Caldwell, C. W. *Biosens. Bioelectron.* **2008**, *23*, 1003−1009.
(11) Masson, J. F.; Battaglia, T. M.; Cramer, J.; Beaudoin, S.; Sierks, M.; Booksh, K. S. *Anal. Bioanal. Chem.* **2006**, *386*, 1951−1959.
(12) Bolduc, O. R.; Pelletier, J. N.; Masson, J. F. *Anal. Chem.* **2010**, *82*, 3699−3706.
(13) Ostuni, E.; Chapman, R. G.; Holmin, R. E.; Takayama, E.; Whitesides, G. M. *Langmuir* **2001**, *17*, 5605−5620.
(14) Wang, F.; Anderson, M.; Bernards, M. T.; Hunt, H. K. *Sensors* **2015**, *15*, 18040−18060.
(15) Konstantinides, S.; Geibel, A.; Olschewski, M.; Kasper, W.; Hruska, N.; Jäckle, S.; Binder, L. *Circulation* **2002**, *106*, 1263−1268.
(16) Maisel, A. *Circulation* **2002**, *105*, 2328−2331.
(17) Ridker, P. M. *Circulation* **2001**, *103*, 1813−1818.
(18) Boriskina, S. V.; Dal Negro, L. *Opt. Lett.* **2010**, *35*, 2496−2498.
(19) Qavi, A. J.; Kindt, J. T.; Gleeson, M. A.; Bailey, R. C. *Anal. Chem.* **2011**, *83*, 5949−5956.
(20) White, I. M.; Oveys, H.; Fan, X.; Smith, T. L.; Zhang, J. *Appl. Phys. Lett.* **2006**, *89*, 191106.
(21) Huckabay, H. A.; Wildgen, S. M.; Dunn, R. C. *Biosens. Bioelectron.* **2013**, *45*, 223−229.
(22) Kim, D. C.; Armendariz, K. P.; Dunn, R. C. *Analyst* **2013**, *138*, 3189−3195.
(23) Ksendov, A.; Lin, Y. *Opt. Lett.* **2005**, *30*, 3344−3346.
(24) Gorodetsky, M. L.; Illchenko, V. S. *J. Opt. Soc. Am. B* **1999**, *16*, 147−154.
(25) Guo, Z.; Quan, H.; Pau, S. *J. Phys. D: Appl. Phys.* **2006**, *39*, 5133−5136.
(26) Riesen, N.; Reynolds, T.; François, A.; Henderson, M. R.; Monro, T. M. *Opt. Express* **2015**, *23*, 28896−28904.
(27) Vernooy, D. W.; Ilchenko, V. S.; Mabuchi, H.; Steed, E. W.; Kimble, H. J. *Opt. Lett.* **1998**, *23*, 247−249.
(28) Gorodetsky, M. L.; Savchenkov, A. A.; Ilchenko, V. S. *Opt. Lett.* **1996**, *21*, 453−455.
(29) François, A.; Himmelhaus, M. *Appl. Phys. Lett.* **2009**, *94*, 031101.
(30) François, A.; Rowland, K. J.; Afshar, S. V.; Henderson, M. R.; Monro, T. M. *Opt. Express* **2013**, *21*, 22566−22577.
(31) Greenspan, P.; Mayer, E. P.; Fowler, S. D. *J. Cell Biol.* **1985**, *100*, 965−973.
(32) François, A.; Riesen, N.; Ji, H.; Afshar, V. S.; Monro, T. M. *Appl. Phys. Lett.* **2015**, *106*, 031104.
(33) Decher, G. *Science* **1997**, *277*, 1232−1237.
(34) Arnold, S.; Khoshsima, M.; Teraoka, I.; Holler, S.; Vollmer, F. *Opt. Lett.* **2003**, *28*, 272−274.
(35) Schweiger, G.; Horn, M. *J. Opt. Soc. Am. B* **2006**, *23*, 212−217.
(36) Lane, S.; West, P.; François, A.; Meldrum, A. *Opt. Express* **2015**, *23*, 2577−2590.
(37) Chen, T.; Hedman, L.; Mattila, P. S.; Jartti, L.; Jartii, T.; Ruuskanen, O.; Soderlund-Venermo, M.; Hedman, K. *PLoS One* **2012**, *7*, 43276.

DOI: 10.1021/acs.analchem.6b00365
Anal. Chem. XXXX, XXX, XXX−XXX